Directing the handedness of helical nanofilaments confined in nanochannels using axially chiral binaphthyl dopants

Sasan Shadpour[†], *Ahlam Nemati*[†], *Jiao Liu*[†], *and Torsten Hegmann*[†,‡,#,*]

[†] Chemical Physics Interdisciplinary Program, Advanced Materials and Liquid Crystal Institute, Kent State University, Kent (OH) 44242-0001, USA; [‡] Department of Chemistry and Biochemistry, Kent State University, Kent (OH) 44242-0001, USA; [#] Brain Health Research Institute, Kent State University, Kent (OH) 44242-0001

KEYWORDS: bent-core liquid crystal, helical nanofilament phase, chirality, confinement, nanochannels, self-assembly

ABSTRACT: In this work, we demonstrate control of the handedness of semi-crystalline modulated helical nanofilaments (HNF_{mod}s) formed by achiral bent-core liquid crystal molecules by axially chiral binaphthyl-based additives as guest molecules solely under spatial nanoconfinement in anodic aluminum oxide nanochannels. The molecules of the same chiral additives are expelled from the HNF_{mod}s in the bulk, and as a result thereof do not affect the handedness or helical pitch of bulk HNF_{mod}s resulting in an HNF_{mod} conglomerate with chirality-preserving growth within each domain. However, under confinement these axially chiral guest molecules, likely embedded in the HNF_{mod} host, do affect the helicity of the HNF_{mod}s. The configuration of the axially chiral molecules decides the HNF_{mod} helix handedness and their concentration the helix angle that is related to helical pitch of HNF_{mod}s. In addition to local imaging data obtained by scanning electron microscopy, global studies by thin film circular dichroism spectropolarimetry support the imaging results.

1. INTRODUCTION

Chirality, defined as the inability to superimpose an object onto its mirror image by any kind of translation or rotation, is omnipresent in nature and of significant relevance in chemistry, physics, materials science, biology, cosmology, and subatomic physics. Ever since Pasteur first demonstrated the conglomerate nature of sodium ammonium tartrate crystals, thereby showing and resolving the enantiomers of tartaric acid,[1] chirality has been a central focus of scientific pursuit. These include for example fabrication methods of nanoscale chiral surfaces, which attracted attention for enhancing enantioselectivity by asymmetric induction,[2] as stationary phase in high-performance liquid chromatography,[3-4] and generally for the amplification of chirality under nanoconfinement.[5-6] Liquid crystals, or more precisely several distinct liquid crystalline phases (nematic, blue, smectic-C, and bent-core liquid crystal phases), are highly sensitive tools to detect chirality and ascertain chirality transfer efficiency,[7-8] bridging length scales from individual molecules to molecular assemblies to nanomaterials to the bulk.[9-11]

Bent-core liquid crystals (BCLCs) are a remarkable topic in soft condensed matter chemistry and physics, especially since the discovery of achiral molecules that can form macroscopically chiral fluids with polar order in tilted layers (SmCP or B2 phase). Another unique BCLC phase is the B4 phase. The B4 phase is a crystalline phase with 'loose' hexatic liquid crystalline ordering, where BCLC molecules self-assemble into helical nanofilaments (HNFs). These HNFs form due to spontaneous symmetry breaking by a mismatch of the achiral molecular halves in smectic layers that is relieved by local saddle-splay, ultimately leading to a limited number (~ 8) of twisted smectic layers.[12] Subtle changes of the molecular shape, for example by introducing an asymmetric core in tris-biphenyl-based BCLCs (*i.e.* one molecular arm is longer than the other one) adds an additional intralayer modulation (HNF_{mod}).[13] By introducing and varying the

position of one or two chiral centers, distinct new morphologies of nanofilaments have been reported, such as dual modulated helical nanofilaments (HNF_{mod2}),[14] helical microfilaments (HμFs),[15] and heliconical layered nanocylinders (HLNCs).[16] All these morphologies are homochiral with the twist sense depending on the configuration of the chiral center(s). However, control over the handedness of such HNFs has been a challenge. Some methods have been proposed to address this challenge such as adding chiral BCLC analogues,[17] employing chiral surfaces,[18] irradiation with circularly polarized light using photoisomerizable molecules,[19] twisted nematic director orientation,[20] or phospholipid chiral layers.[21] However, it is noted that in a binary mixture where HNFs serve as the host, addition of mesogenic, chiral or a range of other guests leads to phase separation in which the guest is expelled into the empty spaces between the HNFs.[22-23] For example, a variety of chiral rod-like (pro-mesogenic) as well as cholesterol-based derivatives, essentially introduced as a chiral dopant for controlling the handedness of HNFs, displayed no observable chiral effect on the proportion of left- and right-handed domains due to low solubility (*i.e*. these additives were expelled) and a significant mismatch in clearing point.[24] We here propose that co-confinement of an achiral HNF host and a chiral guest, particularly when host and guest molecules share a similar molecular (overall bent) shape, should facilitate control over the HNFs' handedness.

The self-assembly of molecules in soft matter is highly sensitive to spatial confinement. The layer undulation in the so-called B7 phase (polarization splay modulated) is suppressed with larger film thickness of such B7 samples.[25] The nematic phase of 5CB (4'-Pentyl-4-biphenylcarbonitrile, serving as a guest phase, can show smectic-like ordering under spatial confinement in the presence of HNFs as a host confined in anodic aluminum oxide (AAO) pores.[26] Certain BCLCs can form either the dark conglomerate (DC) phase or HNFs when

confined in smaller AAO pores, largely due to lower degree of freedom for growth.[27] Contrary, chirality induction in mesoporous organosilica showed that incorporated binaphthyl derivatives are very effective dopants in transferring chirality to the solid state due to the point of attachment and orientation of the chiral axis.[28-29] Considering these facts, we report the successful control of the handedness of HNF_{mod}s using axially chiral additives featuring a commensurate bent-shape when the mixture is confined in nanopores. The homochirality of the resulting nanofilaments is observed by scanning electron microscopy (SEM) and confirmed by circular dichroism (CD) spectropolarimetry.

2. MATERIALS AND METHODS

Figure 1a shows the chemical structures of the tris-biphenyl BCLC as well as the phase sequence and phase transition temperatures.

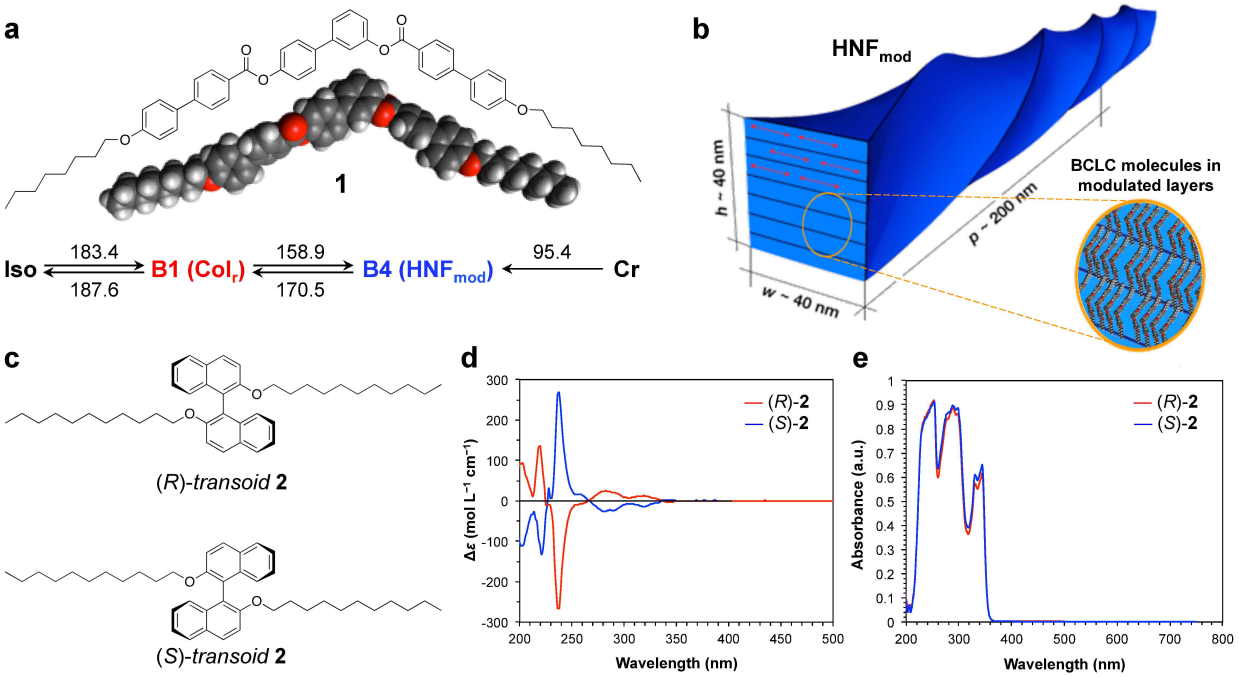

Figure 1. (a) Chemical structure and phase sequence of the BCLC host **1** and (b) morphology and dimensions of the HNF_{mod}s formed by **1**. (c) Chemical structures of the axially chiral binaphthyl guests ((*R*)- and (*S*)-**2**) in their *transoid* conformations. (d) Solution circular dichroism and (e) UV-vis spectra of (*R*)- and (*S*)-**2** recorded in cyclohexane.

Compound **1** forms a rectangular columnar (Col_r or B1) phase over a 14 °C or 17 °C temperature interval on cooling and heating, respectively, and an HNF_{mod} phase over a broad temperature range. The transition from the crystalline phase (Cr) to the Col_r phase is only observed on first heating the recrystallized sample; on cooling the HNF_{mod} phase forms a stable glass.[14] The schematic model of the morphology of these HNF_{mod}s is shown in Figure 1b. Macroscopically the phase is a racemic conglomerate, *i.e*. left- and right-handed homochiral domains form, because the molecules are achiral. The synthesis of the BCLC molecules was described earlier.[14] In our experiments, the HNF_{mod} phase of **1** serves as a host for axially chiral binaphthyl derivatives, (*R*)- and (*S*)-**2**, with undecyloxy aliphatic chains in the 2- and 2'-positions (Figure 1c) as chiral guests. The synthesis of (*R*)- and (*S*)-**2** as well as the spectroscopic characterization (NMR, UV-vis) are described in the Supporting Information (SI, Section 1, Figures S1 – S3). Figures 1c and 1d show the recorded CD and UV-visible spectra of (*R*)- and (*S*)-**2** recorded in cyclohexane. In both spectra the bands visible originate from the binaphthyl moieties and are associated with the ^1B_b transition at 200 to 250 nm, the ^1L_a transition at 250 to 300 nm, and the ^1L_b transition at 300 to 350 nm.[30-31]

In the CD spectra of (*R*)- and (*S*)-**2**, the derivative with (*R*)-configuration shows a positive to negative CD couplet for the ^1B_b transition and positive Cotton effects for the ^1L_a and ^1L_b transition, respectively (and *vice versa* for the derivative with (*S*)-configuration). The exciton coupling theory can interpret the correlation between binaphthyl conformation and CD spectra

based on the dihedral angle,[32-33] which predicts that the (*R*)-configuration of binaphthyl in the CD spectra gives a negative couplet for the dihedral angle between 0° to 100° and that a positive CD couplet is associated with dihedral angles between 110° to 180°.[30, 33-34] Therefore, we can assume that these binaphthyl molecules form *cisoid* conformations in solution (cyclohexane). However, as shown for nematic LC hosts, in the layers of the B4 HNF_{mod} phase, the *transoid* conformation more closely mimics a rod-like molecular shape and would likely be favored.[30-31, 35]

3. RESULTS AND DISSCUSION

At first, the thermal properties of neat **1** and **1** doped with (*R*)- or (*S*)-**2** were studied by differential scanning calorimetry (DSC) as shown in the SI (Section 2, Figure S4). Neat compound **1** shows the phase sequence as well as phase transition temperatures and -enthalpies reported previously.[14] In contrast, the addition of (*R*)- and (*S*)-**2** leads to broader phase transitions (peak broadening in the DSC thermograms), especially on heating, and a decrease in the phase transition temperatures. Noteworthy, there are no additional peaks on heating ((*R*)- and (*S*)-**2** are viscous liquids at room temperature) and no change in the phase sequence of **1**, except for a small additional peak on cooling for the transition from the Col_r to the HNF_{mod} phase (at about 163 °C) that is likely related to inhomogeneities caused by the phase-separated (*R*)- or (*S*)-**2** molecules (SI, Figure S4b).

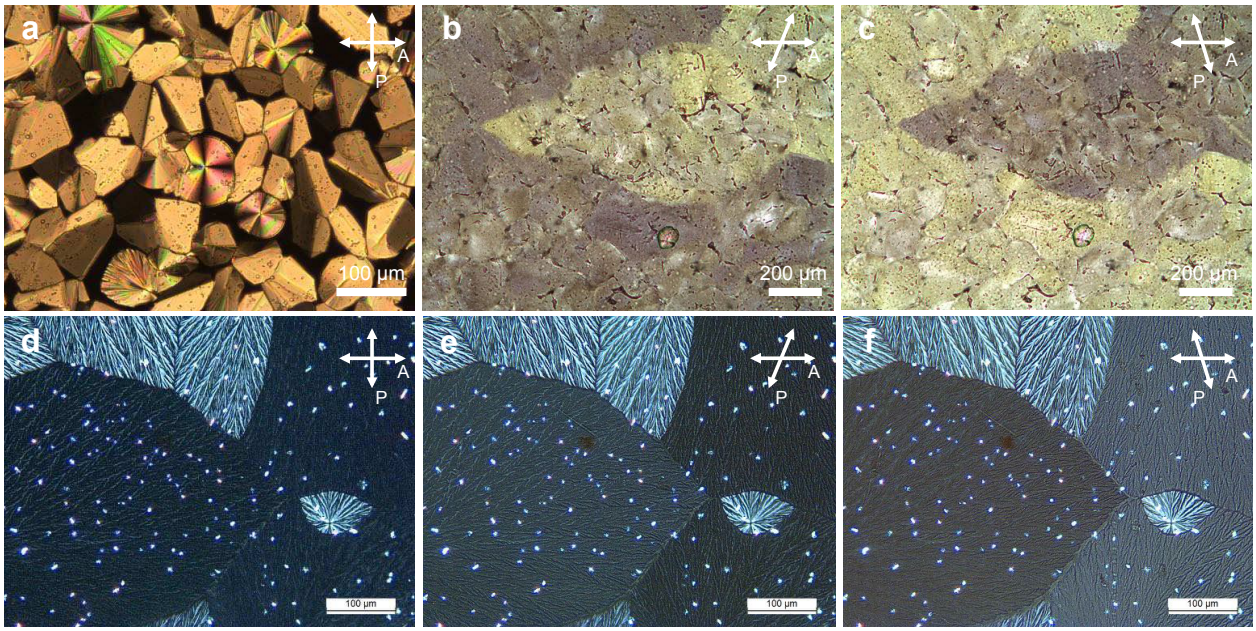

Figure 2. (a – c) Polarized optical photomicrographs of neat **1** (crossed and decrossed polarizer and analyzer; heating/cooling rate: 5 °C min^{-1}): (a) Col_r phase at 182 °C on cooling, (b) HNF_{mod} phase at 25 °C on cooling, and (c) HNF_{mod} phase at 25 °C on cooling. (d – f) **1** containing (*R*)-**2** as chiral guest material at 20 wt.% (crossed and decrossed polarizers and analyzers): HNF_{mod} phase at 25 °C on cooling. The white dots in images (d – f) show the expelled chiral additive (*R*)-**2**. Images for **1** containing (*S*)-**2** are practically identical.

Temperature controlled polarized optical microscopy (POM) images using both crossed and decrossed polarizers for neat **1** (Figures 2a-c) show textures representative of the phase sequence on cooling (Iso – Col_r – HNF_{mod}) established earlier by small-angle X-ray diffraction.[13-14] The images for a mixture of **1** with (*R*)-**2** (Figures 2d-f) show that the chiral guest phase-separates in the bulk, especially at higher concentrations such as at 20 wt.%. These images also show that **1**, neat or doped, forms a chiral conglomerate characterized by equal portions of homochiral domains. Since these domains are reasonably large (often several hundred micrometers across), we captured multiple images from one sample of the mixture of **1** with 20 wt.% (*R*)-**2** and

stitched these images together (SI, Section S4, Figure S5) to show that indeed equal portions of roughly equal-sized homochiral domains are formed. On cooling, the Col_r phase is observed (Figure 2a) followed by the HNF_{mod} phase. The homochiral domains are optically distinguishable by decrossing the polarizers, showing noticeable different birefringence in the heterochiral domains. As reported, HNFs as hosts when mixed with rod-like LC guest molecules form a nanoporous network where guests are expelled, filling the space between adjacent HNFs or bundles of HNFs, overall forming a structure that is phase-separated at the nanoscale.[22-24] As these binary mixture cool down from the isotropic liquid phase, they undergo first-order transitions with random nucleation sites,[36] in which the HNFs, chirality-preserving, grow radially outward with either left- or right-handedness.[37-38]

POM photomicrographs of the binary mixture of **1** doped with 20 wt.% of (*R*)-**2** clearly show that phase separation of the chiral additive occurs as indicated by the bright dots (phase-separated domains in Figures 2d-f; identical observations were made for (*S*)-**2**). Most importantly, Figures 2e and 2f show the alternating handedness of the spherulitic domains after decrossing polarizer and analyzer, thereby producing alternating birefringence changes between the domains with opposite handedness. Hence, (*R*)- and (S)-**2** are expelled, forming phase-separated domains as the HNF_{mod}s grow from nucleation sites, irrespective of the chiral bias (configuration of the axially chiral binaphthyl additives). Photomicrographs shown in Figure S6 (SI, Section S4) show that the size of the roughly spherical domains formed by the expelled (*S*)-**2** is ~ 20 μm in diameter.

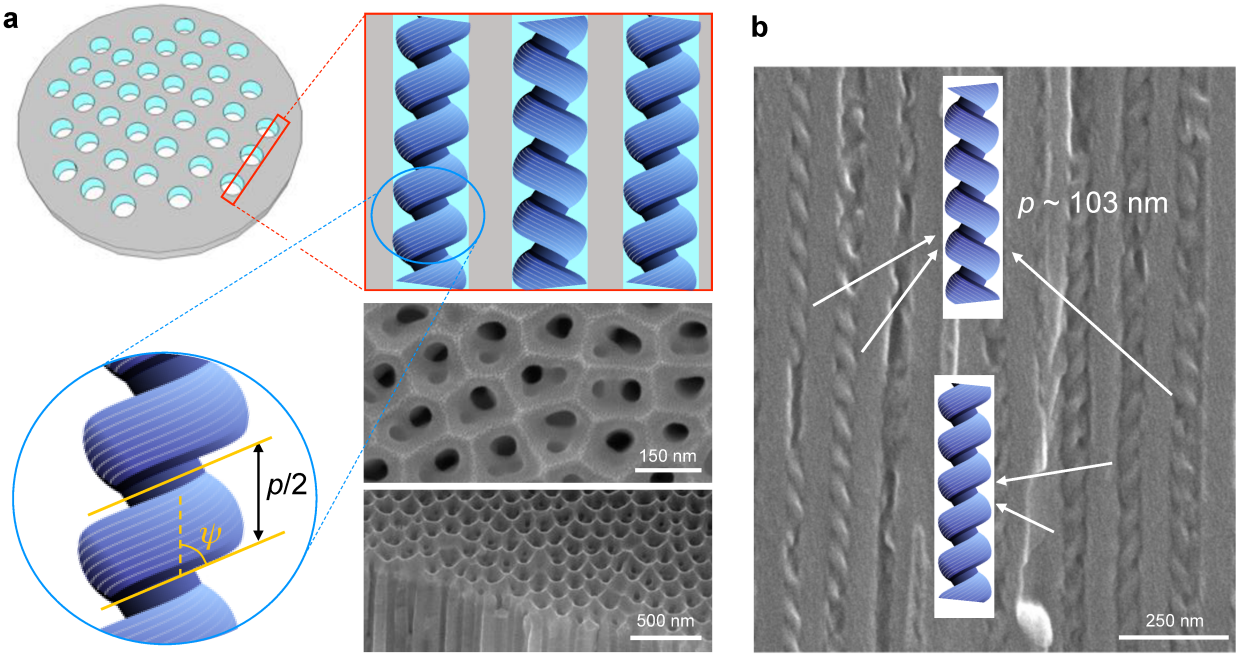

Figure 3. (a) Model of the anodic aluminum oxide (AAO) featuring 60 nm channels with confined HNFs of neat **1** forming with either handedness. Here, $^{p}/_{2}$ is the half-pitch of the helical filaments and ψ the helix angle (for neat **1**: ψ = 45 ± 2°). SEM images show top and angled top views of an empty AAO wafer, respectively. (b) SEM image of HNFs in AAO with 60 nm channel width filled with HNF_{mod}s of either handedness formed randomly in each nanochannel.

One of the most versatile approaches to template-assisted self-assembly of soft-matter nanostructures is the confinement in nanochannels of anodic aluminum oxide (AAO) films as tunable nanoporous media.[39-41] Yoon *et al*. reported on the self-assembly of HNFs in different pore sizes of AAO wafers and proposed a dependency of the AAO pore diameter (d_{AAO}) on the morphology of nanoconfined HNFs, which is 0.7 $w_{bulk} < d_{AAO} < 2\ w_{bulk}$, where w_{bulk} is the width of non-confined HNFs in the bulk (measured by electron or atomic force microscopy), to have an individual HNF in each channel.[42] A model of this self-assembly of HNFs in such AAO channels is shown in Figure 3a. Additionally, it was noted that as d_{AAO} increases, the angle between HNF

ribbons and HNF's long axis (ψ) increases as well. Here, we have chosen AAO with 60 nm pore size diameter to individualize HNF_{mod}s. A representative SEM image of **1** in such 60 nm AAO channels is given in Figure 3b. The values obtained for the helical pitch (p = 200 ± 2 nm) and helix angle (ψ = 45 ± 1°) match the values determined for the non-confined HNF_{mod}s of p ~ 200 nm and ψ ~ 30 to 50°.[42]

Nucleation in the HNF phases starts from isolated sites and progresses through the thin sample while preserving the same handedness within each domain, but alternating from one domain to another.[37] However, the growth of HNFs confined in AAO pores should be very fast considering the inherent temperature gradient (the top is colder than the bottom), *i.e.* progressing from the top to the bottom of the AAO film, although the thermal conductivity of Al_2O_3 is one of the highest for nonmetallic materials,[43] which should make these film almost isothermal. In practice, neat **1** is initially placed on the top of the AAO film (or wafer) and placed on a hot stage. As soon as the temperature reaches the clearing point, the material is sucked into the pores by capillary forces. By slowly decreasing the temperature, for example at a rate of 5 °C min^{-1}, HNF nucleation starts from the colder topside of the sample due to the temperature gradient. The bulk of the material on the top impacts the HNF handedness and chirality-preserving growth into the pores (bulk effect). To eliminate this effect on the nucleation, residual bulk material was continuously and meticulously removed after both an initial as well as a second heating/cooling cycle. Subsequently, the nucleation of the HNFs within the AAO pores occurs in each individual AAO pore during each subsequent heating/cooling cycle rather than being affected by the bulk of the material on the top of the AAO nanoporous template.[42] As a result thereof, all AAO templates (considering multiple AAO samples, several SEM images per AAO template, and ~20 nanopores each) are more or less randomly filled with HNF_{mod}s of either handedness (variance ≤ 5%).

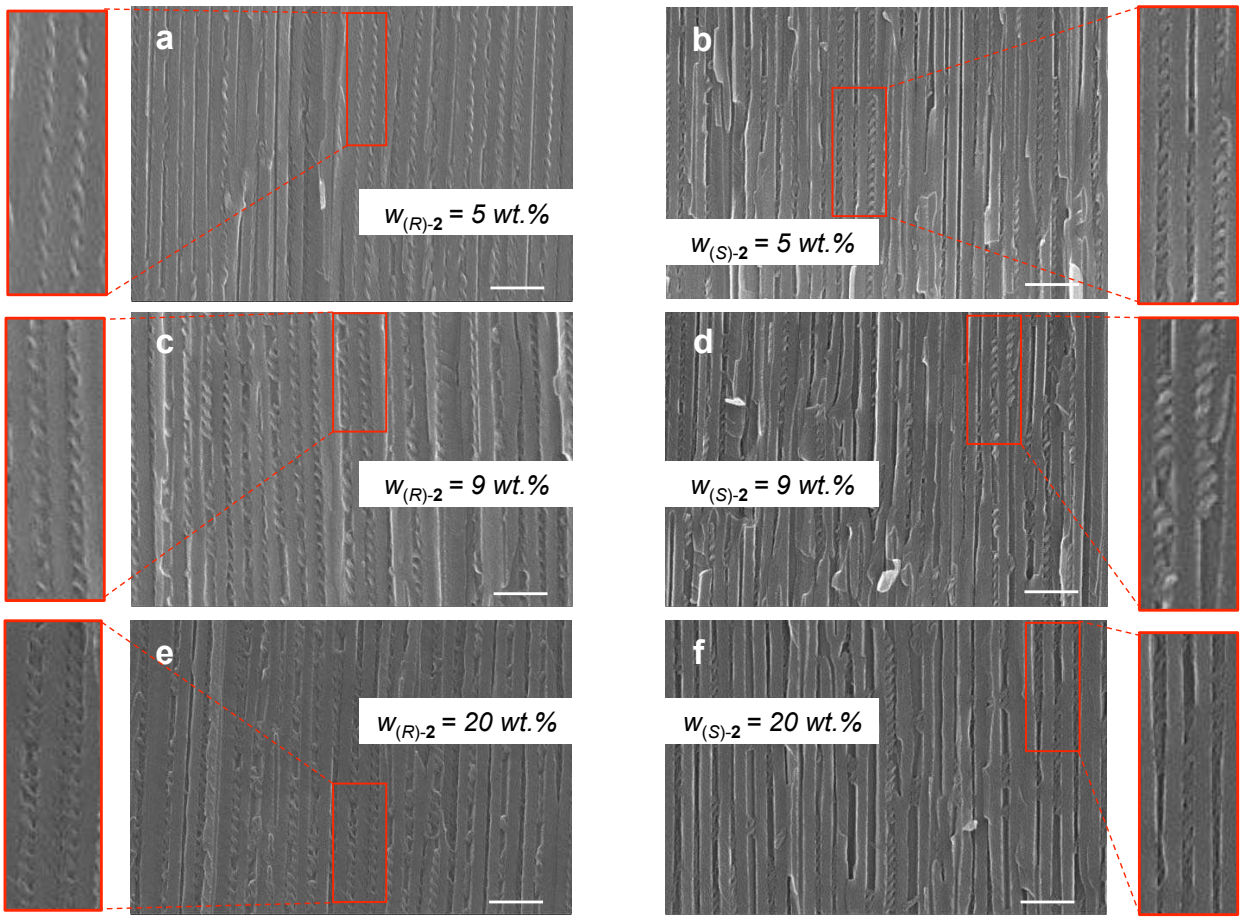

Figure 4. SEM images of **1** with different concentrations (as indicated in each image by weight percentage) of the axially chiral binaphthyl guests: (a, c, and e) with added (*R*)-**2** and (b, d, and f) with added (*S*)-**2** at 5, 9 and 20 wt.%, respectively. Scale bars = 300 nm.

Figure 4 shows the SEM images of the binary mixtures of **1** with different concentrations of (*R*)- and (*S*)-**2**. As confirmed by the SEM images, the configuration of the axially chiral additives clearly directs or induces a specific handedness of the HNF_{mod}s when the mixtures are confined inside the 60 nm AAO pores. Three different concentrations of (*R*)- and (*S*)-**2** have been examined to determine the effectiveness (or efficiency) of these chiral additives to induce one handedness over the other, and potentially induce HNF_{mod}s with shorter pitch p (smaller helix angle ψ). As described earlier, addition of (*R*)- and (*S*)-**2** does not alter p or ψ with increasing

concentration in **1** because they phase-separate in the bulk. Figures 4a, 4c and 4e show SEM images of **1** with (*R*)-**2** at three different concentrations (5, 9 and 20 wt.%) within AAO pores and clearly demonstrate the exclusive formation of left-handed HNF_{mod}s under confinement (at least two independent samples, multiple SEM images of different regions with ~ 20 nanopores each; variance = 0%). Conversely, SEM images of **1** with the identical concentrations (*S*)-**2** exclusively show right-handed HNF_{mod}s. While the dihedral angle and handedness of binaphthyl derivatives can be tuned with various stimuli, such as light irritation[44] or temperature,[45] here they affect the helical sense and with increasing concentration the helix angle ψ (*i.e.* p decreases with increasing w of (*R*)- and (*S*)-**2**). Image analysis reveals that ψ (p) decreases from 32 ± 1° (125 ± 2 nm) for the 5 wt.% mixtures to 29 ± 2° (112 ± 3 nm) for the 9 wt.% mixtures to 27 ± 1° (95 ± 2 nm) for the 20 wt.% mixture. Here it is worth to highlight that standard deviations particularly among reasonably well-formed nanofilaments is quite small (1 – 3° for ψ and 2 – 5 nm for p), indicating that the HNF_{mod}s forming within the AAO nanochannels are relatively uniform in size and shape. The addition of at least 5 wt.% of (*R*)- or (*S*)-**2** turned out to be the lower limit that leads to the exclusive formation of HNF_{mod}s with just one handedness. Reducing the amount of (*R*)- or (*S*)-**2** to even just 4 wt.% results in the formation of both left- and right-handed filaments with no significant bias toward either handedness (SI, Section S5, Figure S7). The effects of the concentration of the chiral additives (*R*)- and (*S*)-**2** with respect to the formation of either a conglomerate or homochiral HNF_{mod}s as well as the helix pitch and helix angle are graphically summarized in Figure 5. Of course, p and ψ are geometrically related, but the almost linear relationship between the concentrations of (*R*)- or (*S*)-**2** and p (or ψ) throughout the homochiral regime (yellow highlighted area) now allows for a selection of the precise amount of (*R*)- or (*S*)-**2** needed to attain a particular handedness as well as value of p (or ψ).

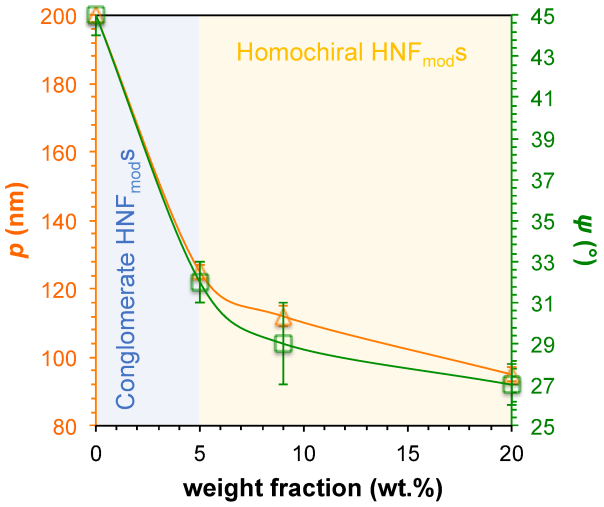

Figure 5. Plot of the dependencies of helix pitch (p) and helix angle (ψ) of the HNF$_{mod}$s formed within AAO nanopores on the concentration of the axially chiral additives (*R*)- and (*S*)-**2**.

Chen *et al*. studied a wide range of binary mixtures of chiral additives with NOBOW (forming the B4 HNF phase) and reported that, with few exceptions and for very high concentration of chiral dopant, there is no effects on induced handedness of HNFs in most cases due to low solubility and the high temperature clearing point.[24] To highlight the role of the chiral additive's molecular shape, ideally commensurate to the BCLC host, we also performed identical experiments with a cholesterol-based derivative, cholesteryl oleyl carbonate (COC) doped at various concentrations into **1** and confined to AAO pores (SI, Section S5, Figure S8). The SEM images clearly demonstrate that COC does not impact of the HNF$_{mod}$s' helicity inside the AAO pores. In fact, both types of handedness are observed and form randomly within one and the same AAO wafer. Thus, we assume that a combination of commensurate molecular shape and axial chirality of **2** under confinement of the mixture play the key roles in directing the HNF$_{mod}$ helical sense. To further support this argument, we also performed the same experiments with 10 wt.% of another chiral additive. R811, a rod-like compound featuring a phenylbenzoate core and two aliphatic side chains (the side chain containing the chiral center is attached *via* an ester

linkage), should structurally be considered more closely related to structure of the side arms of **1** especially when compared to **2** or COC. However, just like COC, R811 phase-separates within the AAO pores. SEM imaging clearly shows HNF_{mod}s with either handedness, randomly distributed within one and the same AAO template, and no induction of just one or the other handedness (SI, Section S5, Figures S9a and 9b; for the chemical structure see Figure S9c).

To emphasize that the induction of the HNF_{mod} helical sense by (*S*)- or (*R*)-**2** works strictly under confinement, a single AAO wafer was divided into two segments using Kapton tape. Two mixtures, one containing 20 wt.% (*R*)-**2** and the other one 20 wt.% (*S*)-**2**, were separately melted down into the AAO pores on each side of the tape, and the resulting AAO sample twice heated and subsequently cooled. The residual bulk materials were meticulously wiped off as described earlier, and the sample was again heated above the clearing point of the mixtures and then slowly cooled down to avoid the bulk effect (Figure 6a).

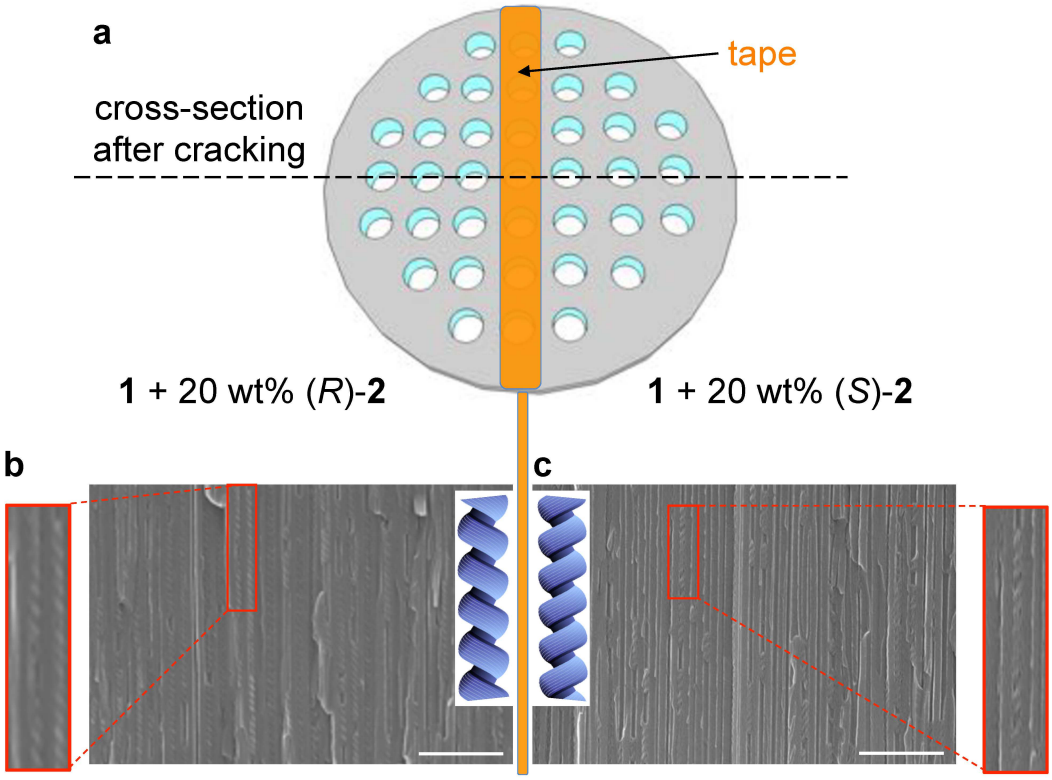

Figure 6. (a) AAO wafer divided into two segments by Kapton tape and two binary mixtures, **1** + 20 wt.% (*R*)-**2** and **1** + 20 wt.% (*S*)-**2**, confined on each side of the tape. (b) SEM image for **1** + 20 wt.% (*R*)-**2** in AAO (60 nm pore diameter) forming again exclusively left-handed HNF_{mod}s and (c) SEM image for **1** + 20 wt.% (*S*)-**2** in AAO (60 nm pore diameter) forming again exclusively right-handed HNF_{mod}s. Scale bars = 500 nm.

The cross-sectional SEM images of this subdivided AAO film show the expected HNF_{mod} helicity on either side matching with the helicity shown in Figure 4, with p and ψ at identical values of the 20 wt.% in **1** sample shown in Figures 4e and 4f (Figures 6b and 6c).

To further support the imaging data, we also performed thin film circular dichroism (CD) experiments. CD spectropolarimetry of the various B4 filament morphologies has previously been reported.[14-15, 46] To eliminate the correlation between dichroism and birefringence of the LC molecules, all samples and sample areas were investigated at numerous sample rotation angles. The spectra were then summed up to provide genuine CD signals of the sample areas. The area interrogated by the light beam and detector is ~ 0.4 cm in diameter (this is almost the diameter of the AAO wafer) and is comparable to the typical size of domains in bulk thin film HNF phases.

The schematic of the setup to collect these CD spectra of HNF_{mod}s confined in AAO pores is shown in Figure 7a. It is important to note that the HNF_{mod}s' helical axes are all aligned parallel to the light beam and thus CD interrogates the handedness of the filaments directly. Nevertheless, non-zero contributions of birefringence and linear dichroism still need to be cancelled out, which is achieved by rotating the sample and averaging (or summing up) the obtained tin film CD spectra. The neat sample of **1** then shows CD spectra with both positive and negative signs (Figure 7b). The sum spectrum is not zero with respect to the measured ellipticity (although low in intensity), which reflects that the beam by chance most certainly interrogates

more domains of one handedness than the other one. Relocating the sample just slightly produces a sum-CD signal that is again non-zero, also low in intensity, but somewhat opposite in sign across multiple wavelength ranges, but especially in the lower wavelength region from 300 to 600 nm (SI, Section S6, Figure S10). This further supports the earlier argument that, on average, neat **1** forms roughly equal portions of left- and right-handed HNF_{mod}s within AAO nanopores. The bulk thin film spectra for the binary mixtures of **1** with either (*R*)-**2** or (*S*)-**2** between two quartz substrates are shown in the SI (Section S6, Figure S11). This result (*i.e.* both positive and negative CD bands) supports the POM observations (Figure 2d-f) showing domains with either handedness. Clearly, there are domains with different handedness corresponding to a different sign of the CD bands and chiral additive molecules forming phase-separated domains that do not impact the CD signals, especially at wavelengths above 300 nm, where (*R*)- and (*S*)-**2** show only weak CD intensity and all the signal is caused by the HNF_{mod}s formed by **1**.

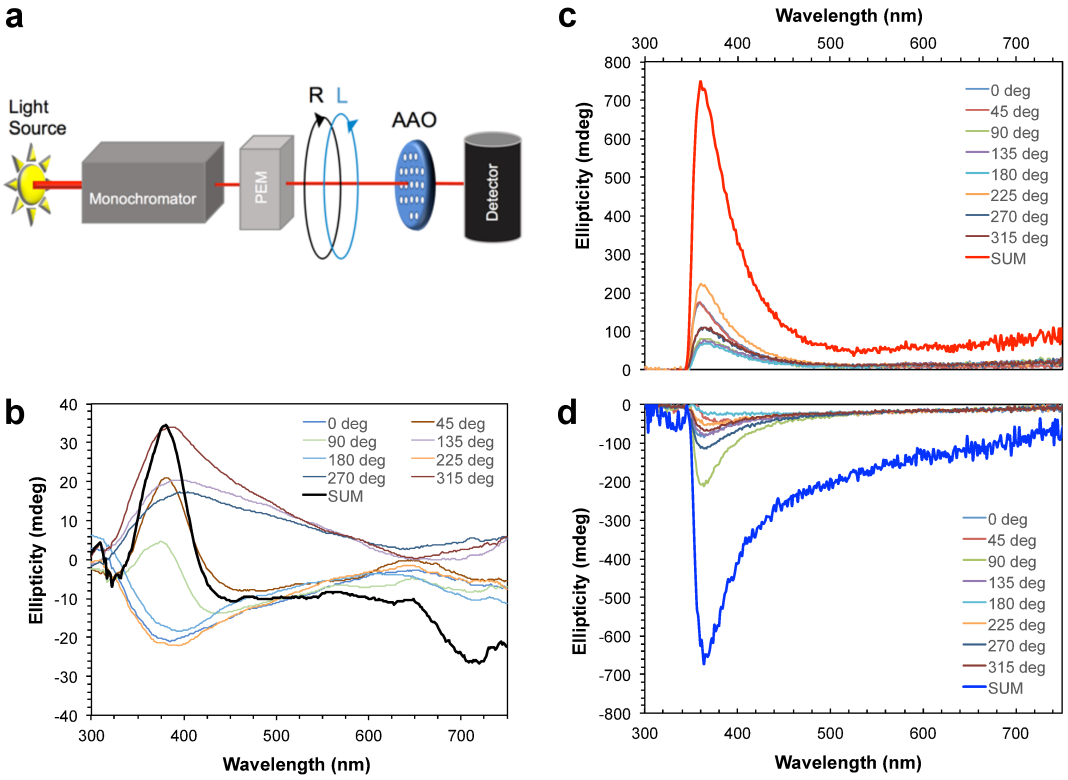

Figure 7. (a) Schematic setup of the CD experiment and the position of HNF_{mod}s in AAO. Thin film CD spectra of: (b) **1** in AAO, (c) **1** + 20 wt.% (*R*)-**2**, and (d) **1** + 20 wt.% (*S*)-**2**. Thin film CD spectra of **1** + 5 wt.% and **1** + 9 wt.% of (*R*)-**2** are shown in the SI (Section S6, Figure S12).

In contrast, the CD spectra of the mixtures confined inside the AAO pores (Figures 7c and 7d for the 20 wt.% (*R*)- and (*S*)-**2** samples as well as Figures S12a and S12b for the 5 and 9 wt.% (*R*)-**2** samples, respectively), show exclusively positive (for **1** + (*R*)-**2**) or negative CD bands (for **1** + (*S*)-**2**) supporting both the SEM and the POM data regarding the handedness of the induced HNF_{mod}s. Characteristically, the sum CD bands for each mixture, differing only in the configuration of the axially chiral guest show, as expected, equal and comparatively higher intensities considering the identical sample thickness given by the AAO wafers.

3. CONCLUSION

In conclusion, we demonstrate an efficient approach to control the handedness of HNFs by the addition of the two enantiomers of an axially chiral guest under confinement in nanopores. Limiting phase separation under spatial nanoconfinement coupled with the ability of the axially chiral binaphthyl derivatives to adjust shape (*i.e.* dihedral angle), when embedded in liquid crystalline phases such as the twisted-smectic layers of HNF_{mod}s, allows this particular type of chiral additive to dictate both the HNF_{mod} handedness and the helical pitch. The possibility for commensurate bent shapes of chiral guest (although other conformations cannot be fully excluded) and achiral host (SI, Section S7, Figure S13), unlike for both the cholesterol- and the rod-like phenylbenzoate-based chiral additives, facilitates interactions among guest and host molecules (sergeant-soldier effect), but only under confinement. Another possible scenario to explain the effect of (*R*)- and (*S*)-**2** on the formation of homochiral HNF_{mod}s within the AAO

nanopores could be that these chiral additives (as a liquid over the entire temperature range from the isotropic liquid state of **1** to room temperature) solvates the growing filaments to some degree, acting as a chiral solvent under these confinement conditions. However, at the temperature compound **1** starts forming HNF_{mod}s on cooling (at ~ 160 °C), (*R*)- and (*S*)-**2**, COC as well as R811 are all isotropic liquids and should similarly act as phase-separated chiral solvent. Since only the axially chiral derivatives described here affect handedness and helix pitch (helix angle), we assume that the molecular shape of the chiral additive does play a role and that these axially chiral additives are, at least in part, embedded. Future work that will interrogate structurally related, axially chiral additives will focus on deciphering these hypotheses. Chiral additives (mostly rod-like chiral derivatives) are largely expelled from these nanofilaments in the bulk likely due to molecular incompatibility with the crystalline packing of the bent-core molecules within the filaments' twisted layers. Hence, the described approach of using confinement to control chirality transfer, absent in the bulk, bodes well for a variety of applications in chiral separation and the use of these nanofilaments as chiral templates for a range of nanomaterials, particularly with a focus on plasmonic chiral superstructures and circularly polarized emission from helically assembled quantum dots, with prescribed uniform handedness and helix angle (*i.e.* helical pitch) under confinement.

ASSOCIATED CONTENT

Supporting Information

The Supporting Information is available free of charge at …

Materials and methods, synthesis and characterization of (*R*)- and (*S*)-**2**, DSC data, additional POM images, SEM images and CD spectra, conformational analysis data for compounds **1** as well as (*R*)- and (*S*)-**2**.

AUTHOR INFORMATION

Corresponding Author

*E-mail: thegmann@kent.edu. Phone: +1 (330) 672-7770

ORCID

Author Contributions

S.S., A.N., and J.L. performed the synthesis, A.N. the CD studies, and S.S. the POM as well as SEM studies. T.H. directed the study. S.S. and T.H. with contributions from all co-authors wrote the manuscript.

Funding Sources

The work was financially supported by the U.S. National Science Foundation (NSF, DMR-1506018), the Ohio Third Frontier program for Ohio Research Scholars "Research Cluster on Surfaces in Advanced Materials", which also supports the Liquid Crystal Characterization facility at the Advanced Materials and Liquid Crystal Institute (KSU), where some of the current SEM data were acquired.

Notes

The authors declare no competing financial interest.

ACKNOWLEDGMENT

We acknowledge Dr. Dong Ki Yoon for fruitful discussions.

ABBREVIATIONS

BCLC, bent-core liquid crystal; LC, liquid crystal; UV, ultraviolet; CD, circular dichroism; SEM, scanning electron microscopy; AAO, anodic aluminum oxide; HNF, helical nanofilament; Sm phase, smectic phase; DC, dark conglomerate.

REFERENCES

1. Pasteur, L., Sur les relations qui peuvent exister entre la forme crystalline, la composition chimique et le sens de la polarization rotatoire. *Annales Chimie Phys*. **1848**, *24*, 442-459.

2. Brunet, E., Asymmetric induction under confinement. *Chirality* **2002**, *14*, 135-143.

3. Francotte, E. R., Enantioselective chromatography as a powerful alternative for the preparation of drug enantiomers. *J. Chromatogr. A* **2001**, *906*, 379-397.

4. Gübitz, G., Separation of drug enantiomers by HPLC using chiral stationary phases—a selective review. *Chromatographia* **1990**, *30*, 555-564.

5. Cao, H.; De Feyter, S., Amplification of chirality in surface-confined supramolecular bilayers. *Nature communications* **2018**, *9*, 3416.

6. Seibel, J.; Verstraete, L.; Hirsch, B. E.; Braganca, A. M.; De Feyter, S., Biasing enantiomorph formation via geometric confinement: nanocorrals for chiral induction at the liquid-solid interface. *J. Am. Chem. Soc*. **2018**, *140*, 11565-11568.

7. Solladié, G.; Zimmermann, R. G., Liquid Crystals: A tool for studies on chirality. *Angew. Chem. Int. Ed*. **1984**, *23*, 348-362.

8. Ohzono, T.; Yamamoto, T.; Fukuda, J.-i., A liquid crystalline chirality balance for vapours. *Nat. Commun.* **2014**, *5*, 3735.

9. Nemati, A.; Shadpour, S.; Querciagrossa, L.; Li, L.; Mori, T.; Gao, M.; Zannoni, C.; Hegmann, T., Chirality amplification by desymmetrization of chiral ligand-capped nanoparticles to nanorods quantified in soft condensed matter. *Nat. Commun.* **2018**, *9*, 3908.

10. Shadpour, S.; Vanegas, J. P.; Nemati, A.; Hegmann, T., Amplification of chirality by adenosine monophosphate-capped luminescent gold nanoclusters in nematic lyotropic chromonic liquid crystal tactoids. *ACS Omega* **2019**, *4*, 1662-1668.

11. Eelkema, R.; Feringa, B. L., Amplification of chirality in liquid crystals. *Org. Biomol. Chem.* **2006**, *4*, 3729-3745.

12. Hough, L.; Jung, H.-T.; Krüerke, D.; Heberling, M.; Nakata, M.; Jones, C.; Chen, D.; Link, D. R.; Zasadzinski, J.; Heppke, G., Helical nanofilament phases. *Science* **2009**, *325*, 456-460.

13. Tsai, E.; Richardson, J. M.; Korblova, E.; Nakata, M.; Chen, D.; Shen, Y.; Shao, R.; Clark, N. A.; Walba, D. M., A modulated helical nanofilament phase. *Angew. Chem. Int. Ed.* **2013**, *52*, 5254-5257.

14. Li, L.; Salamonczyk, M.; Jákli, A.; Hegmann, T., A dual modulated homochiral helical nanofilament phase with local columnar ordering formed by bent core liquid crystals: effects of molecular chirality. *Small* **2016**, *12*, 3944-3955.

15. Li, L.; Salamończyk, M.; Shadpour, S.; Zhu, C.; Jákli, A.; Hegmann, T., An unusual type of polymorphism in a liquid crystal. *Nat. Commun.* **2018**, *9*, 714.

16. Shadpour, S.; Nemati, A.; Boyd, N. J.; Li, L.; Prévôt, M. E.; Wakerlin, S. L.; Vanegas, J. P.; Salamończyk, M.; Hegmann, E.; Zhu, C., Heliconical-layered nanocylinders (HLNCs)–hierarchical self-assembly in a unique B4 phase liquid crystal morphology. *Mater. Horizons* **2019**, *6*, 959-968.

17. Thisayukta, J.; Niwano, H.; Takezoe, H.; Watanabe, J., Effect of chiral dopant on a helical Sm1 phase of banana-shaped NnO-PIMB molecules. *J. Mater. Chem.* **2001**, *11*, 2717-2721.

18. Shiromo, K.; Sahade, D. A.; Oda, T.; Nihira, T.; Takanishi, Y.; Ishikawa, K.; Takezoe, H., Finite enantiomeric excess nucleated in an achiral banana mesogen by chiral alignment surfaces. *Angew. Chem. Int. Ed.* **2005**, *44*, 1948-1951.

19. Choi, S. W.; Izumi, T.; Hoshino, Y.; Takanishi, Y.; Ishikawa, K.; Watanabe, J.; Takezoe, H., Circular-polarization-induced enantiomeric excess in liquid crystals of an achiral, bent-shaped mesogen. *Angew. Chem. Int. Ed.* **2006**, *45*, 1382-1385.

20. Choi, S. W.; Kang, S.; Takanishi, Y.; Ishikawa, K.; Watanabe, J.; Takezoe, H., Intrinsic chirality in a bent-core mesogen induced by extrinsic chiral structures. *Angew. Chem. Int. Ed.* **2006**, *45*, 6503-6506.

21. Lee, G.; Carlton, R. J.; Araoka, F.; Abbott, N. L.; Takezoe, H., Amplification of the stereochemistry of biomolecular adsorbates by deracemization of chiral domains in bent-core liquid crystals. *Adv. Mater.* **2013**, *25*, 245-249.

22. Zhu, C.; Chen, D.; Shen, Y.; Jones, C. D.; Glaser, M. A.; Maclennan, J. E.; Clark, N. A., Nanophase segregation in binary mixtures of a bent-core and a rodlike liquid-crystal molecule. *Phys. Rev. E* **2010**, *81*, 011704.

23. Sasaki, Y.; Nagayama, H.; Araoka, F.; Yao, H.; Takezoe, H.; Ema, K., Distinctive thermal behavior and nanoscale phase separation in the heterogeneous liquid-crystal B4 matrix of bent-core molecules. *Phys. Rev. Lett.* **2011**, *107*, 237802.

24. Chen, D.; Tuchband, M. R.; Horanyi, B.; Korblova, E.; Walba, D. M.; Glaser, M. A.; Maclennan, J. E.; Clark, N. A., Diastereomeric liquid crystal domains at the mesoscale. *Nat. Commun.* **2015**, *6*, 7763.

25. Zhang, C.; Gao, M.; de Almeida, R. R.; Weissflog, W.; Lavrentovich, O. D.; Jákli, A., Polarization-modulated bent-core liquid crystal thin films without layer undulation. *Phys. Rev. Lett.* **2019**, *122*, 137801.

26. Kim, H.; Ryu, S. H.; Tuchband, M.; Shin, T. J.; Korblova, E.; Walba, D. M.; Clark, N. A.; Yoon, D. K., Structural transitions and guest/host complexing of liquid crystal helical nanofilaments induced by nanoconfinement. *Sci. Adv.* **2017**, *3*, e1602102.

27. Foley, L.; Park, W.; Yang, M.; Carlson, E.; Korblova, E.; Yoon, D. K.; Walba, D. M., Nanoconfinement of the low-temperature dark conglomerate: Structural control from focal conics to helical nanofilaments. *Chem.–Eur. J.* **2019**, *25*, 7438-7442.

28. MacLean, M. W.; Wood, T. K.; Wu, G.; Lemieux, R. P.; Crudden, C. M., Chiral periodic mesoporous organosilicas: Probing chiral induction in the solid state. *Chem. Mater.* **2014**, *26*, 5852-5859.

29. Jayalakshmi, V.; Wood, T.; Basu, R.; Du, J.; Blackburn, T.; Rosenblatt, C.; Crudden, C. M.; Lemieux, R. P., Probing the pore structure of a chiral periodic mesoporous organosilica using liquid crystals. *J. Mater. Chem.* **2012**, *22*, 15255-15261.

30. Mori, T.; Sharma, A.; Hegmann, T., Significant enhancement of the chiral correlation length in nematic liquid crystals by gold nanoparticle surfaces featuring axially chiral binaphthyl ligands. *ACS Nano* **2016**, *10*, 1552-1564.

31. Nemati, A.; Shadpour, S.; Querciagrossa, L.; Mori, T.; Zannoni, C.; Hegmann, T., Highly sensitive, tunable chirality amplification through space visualized for gold nanorods capped with axially chiral binaphthyl derivatives. *ACS Nano* **2019**, *10*, 10312-10326.

32. Chirality in Liquid Crystals; Kitzerow, H.-S., Bahr, C., Eds.; Springer-Verlag: New York, 2001.

33. Harada, N.; Nakanishi, K. Circular Dichroic Spectroscopy: Exciton Coupling in Organic Stereochemistry; University Science Books: South Orange, NJ, 1983.

34. Proni, G.; Spada, G. P.; Lustenberger, P.; Welti, R.; Diederich, F., Conformational analysis in solution of C2-symmetric 1,1'-binaphthyl derivatives by circular dichroism spectroscopy and cholesteric induction in nematic mesophases. *J. Org. Chem.* **2000**, *65*, 5522-5527.

35. Goh, M.; Park, J.; Han, Y.; Ahn, S.; Akagi, K., Chirality transfer from atropisomeric chiral inducers to nematic and smectic liquid crystals–synthesis and characterization of di-and tetra-substituted axially chiral binaphthyl derivatives. *J. Mater. Chem.* **2012**, *22*, 25011-25018.

36. Nagayama, H.; Sasaki, Y.; Araoka, F.; Ema, K.; Ishikawa, K.; Takezoe, H., Discrete and sequential formation of helical nanofilaments in mixtures consisting of bent-and rod-shaped molecules. *Soft Matter* **2011**, *7*, 8766-8769.

37. Chen, D.; Maclennan, J. E.; Shao, R.; Yoon, D. K.; Wang, H.; Korblova, E.; Walba, D. M.; Glaser, M. A.; Clark, N. A., Chirality-preserving growth of helical filaments in the B4 phase of bent-core liquid crystals. *J. Am. Chem. Soc.* **2011**, *133*, 12656-12663.

38. Takanishi, Y.; Shin, G. J.; Jung, J. C.; Choi, S.-W.; Ishikawa, K.; Watanabe, J.; Takezoe, H.; Toledano, P., Observation of very large chiral domains in a liquid crystal phase formed by mixtures of achiral bent-core and rod molecules. *J. Mater. Chem.* **2005**, *15*, 4020-4024.

39. Shin, K.; Xiang, H.; Moon, S. I.; Kim, T.; McCarthy, T. J.; Russell, T. P., Curving and frustrating flatland. *Science* **2004**, *306*, 76-76.

40. Wu, Y.; Cheng, G.; Katsov, K.; Sides, S. W.; Wang, J.; Tang, J.; Fredrickson, G. H.; Moskovits, M.; Stucky, G. D., Composite mesostructures by nano-confinement. *Nat. Mater.* **2004**, *3*, 816.

41. Dobriyal, P.; Xiang, H.; Kazuyuki, M.; Chen, J.-T.; Jinnai, H.; Russell, T. P., Cylindrically confined diblock copolymers. *Macromolecules* **2009**, *42*, 9082-9088.

42. Kim, H.; Lee, S.; Shin, T. J.; Korblova, E.; Walba, D. M.; Clark, N. A.; Lee, S. B.; Yoon, D. K., Multistep hierarchical self-assembly of chiral nanopore arrays. *Proc. Natl. Acad. Sci. U.S.A.* **2014**, *111*, 14342-14347.

43. Touloukian YS, D. D., *Thermophysical Properties of Matter*. Springer: New York, 1970.

44. Orlova, T.; Lancia, F.; Loussert, C.; Iamsaard, S.; Katsonis, N.; Brasselet, E., Revolving supramolecular chiral structures powered by light in nanomotor-doped liquid crystals. *Nat. Nanotechnol.* **2018**, *13*, 304.

45. Roszak, K.; Katrusiak, A., High-pressure and temperature dependence of the spontaneous resolution of 1, 1′-binaphthyl enantiomers. *Phys. Chem. Chem. Phys.* **2018**, *20*, 5305-5311.

46. Niwano, H.; Nakata, M.; Thisayukta, J.; Link, D. R.; Takezoe, H.; Watanabe, J., Chiral memory on transition between the B2 and B4 phases in an achiral banana-shaped molecular system. *J. Phys. Chem. B* **2004**, *108* (39), 14889-14896.

TOC Figure: